PROCEEDINGS OF SCIENCE

The femtoscopic technique—an invaluable tool in studies of exotic hadrons

Zhi-Wei Liu,[a] **Jun-Xu Lu**[a] **and Li-Sheng Geng**[a,b,c,d,e,*]

[a] *School of Physics, Beihang University, Beijing 102206, China*
[b] *Centrale Pekin, Beihang University, Beijing 100191, China*
[c] *Peng Huanwu Collaborative Center for Research and Education, Beihang University, Beijing 100191, China*
[d] *Beijing Key Laboratory of Advanced Nuclear Materials and Physics, Beihang University, Beijing 102206, China*
[e] *Southern Center for Nuclear-Science Theory (SCNT), Institute of Modern Physics, Chinese Academy of Sciences, Huizhou 516000, Chin*

E-mail: lisheng.geng@buaa.edu.cn

The femtoscopic technique has emerged as an invaluable tool in probing the strong interactions between pairs of stable and unstable particles. This presentation stresses that it can contribute uniquely to understanding the many candidates of exotic hadrons discovered since 2003. The essential idea is to check the molecular picture for these exotic hadrons by extracting the strong interactions between their constituents. We show first how the general features of the strong interactions manifest themselves in the femtoscopic correlation functions and then we demonstrate the proposed strategy by taking the $D_{s0}^*(2317)$, the pentaquark states, $P_c(4457)$ and $P_c(4440)$, and the tetraquark states $Z_c(3900)$ and $Z_{cs}(3985)$ as concrete examples.

10th International Conference on Quarks and Nuclear Physics (QNP2024)
8-12 July, 2024
Barcelona, Spain

*Speaker

PoS(QNP2024)044

1. Introduction

Traditionally, hadron-hadron interactions have been studied based on scattering experiments, first pioneered by Sir Ernest Rutherford, who discovered that atoms have a core, the nucleus [1]. Using such techniques, we have learned a lot about the nuclear force. However, conventional scattering experiments are difficult or even impossible for unstable particles because of their short lifetime and the lack of suitable targets and high-quality beams. In the last few years, femtoscopy, which measures two particle momentum correlation functions in high-energy proton-proton (pp), proton-nucleus (pA), and nucleus-nucleus (AA) collisions, has made remarkable progress in probing the strong interactions between various pairs of hadrons [2].

In the conventional or naive quark model of Gell-mann and Zweig, mesons are composed of a pair of quark and antiquark and baryons are made up of three quarks [3, 4]. Such a picture works extremely till about 2003. This year, two hadrons that do not easily fit into the naive quark model, i.e., $X(3872)$ and $D_{s0}^*(2317)$ [5–7], were discovered, ushering into a new era of hadron physics and the non-perturbative strong interaction. After 2003, many such states were discovered, including the tetraquark states $Z_c(3900)/Z_{cs}(3985)$ [8, 9], the pentaquark states $P_c(4312)$, $P_c(4440)$, and $P_c(4457)$ [10]. See the review of particle physics for a complete list of such states [11]. Because most (if not all) of these states are located close to the mass thresholds of pairs of conventional hadrons, they have been conjectured to be hadronic molecules, similar to the deuteron composed of a proton and a neutron. Many ways have been proposed to verify the molecular nature, such as searching for missing symmetry partners [12] and three-hadron molecules [13]. If one can extract the strong interactions between the constituents of an exotic hadron, it will help verify the molecular conjecture. For such a purpose, the femtoscopic technique can be an invaluable tool [14].

2. Femtoscopic correlation functions

The femtoscopic correlation function is defined as the ratio of the Lorentz-invariant two-particle spectrum to the product of single-particle inclusive momentum spectra [15, 16],

$$C(\boldsymbol{p}_1, \boldsymbol{p}_2) = \frac{E_1 E_2 \mathrm{d}N_{12}/(\mathrm{d}^3 p_1 \mathrm{d}^3 p_2)}{(E_1 \mathrm{d}N_1/\mathrm{d}^3 p_1)\cdot(E_2 \mathrm{d}N_2/\mathrm{d}^3 p_2)} = \frac{P(\boldsymbol{p}_1, \boldsymbol{p}_2)}{P(\boldsymbol{p}_1)\cdot P(\boldsymbol{p}_2)}, \tag{1}$$

where $\boldsymbol{p}_i$ $(i = 1, 2)$ is the momentum of each particle, and E_i $(i = 1, 2)$ is the energy of particle i. Experimentally, the correlation function is obtained using the mixed-event technique [2], which is computed as,

$$C(k) = \mathcal{N}\frac{N_{\mathrm{same}}(k)}{N_{\mathrm{mixed}}(k)}, \tag{2}$$

where the relative momentum of two particles $k = |\boldsymbol{p}_1 - \boldsymbol{p}_2|/2$, $N_{\mathrm{same}}(k)$ and $N_{\mathrm{mixed}}(k)$ represent the same and different event k distributions, respectively. The normalization constant $\mathcal{N}$ denotes the corrections of experimental effects. Theoretically, the two-particle momentum correlation function

can be computed by the Koonin–Pratt (KP) formula [15, 17],

$$C(\boldsymbol{p}_1, \boldsymbol{p}_2) = \frac{\int \mathrm{d}^4x_1\mathrm{d}^4x_2\ S_1(x_1, \boldsymbol{p}_1)S_2(x_2, \boldsymbol{p}_2)\ |\Psi^{(-)}(\boldsymbol{r}, \boldsymbol{k})|^2}{\int \mathrm{d}^4x_1\mathrm{d}^4x_2\ S_1(x_1, \boldsymbol{p}_1)S_2(x_2, \boldsymbol{p}_2)} \tag{3a}$$

$$\simeq \int \mathrm{d}\boldsymbol{r}\ S_{12}(r)\ |\Psi^{(-)}(\boldsymbol{r}, \boldsymbol{k})|^2, \tag{3b}$$

where $S_i(x_i, \boldsymbol{p}_i)$ $(i = 1, 2)$ is the single-particle source function of particle i. $\Psi^{(-)}$ denotes the relative wave function with the relative coordinate $\boldsymbol{r}$ and momentum $\boldsymbol{k}$, in which the final-state interactions are incorporated. For a non-identical two-particle system experiencing only strong interactions, the relative wave function in the two-body outgoing state can be written as,

$$\Psi_S^{(-)}(\boldsymbol{r}, \boldsymbol{k}) = e^{i\boldsymbol{k}\cdot\boldsymbol{r}} - j_0(kr) + \psi_0(r, k), \tag{4}$$

where the spherical Bessel function j_0 represents the $l = 0$ component of the non-interacting wave function, and ψ_0 denotes the $l = 0$ scattering wave function affected by the strong interaction. Substituting the relative wave function (4) into the KP formula, the correlation function is simplified into the following form

$$C(k) \simeq 1 + \int_0^\infty 4\pi r^2\mathrm{d}r\ S_{12}(r)\ \left[|\psi_0(r, k)|^2 - |j_0(kr)|^2\right]. \tag{5}$$

3. General features of femtoscopic correlation functions for strong interactions of various strengths

Depending on its strength, an attractive interaction can generate either a deeply bound state, a weakly bound state, a virtual state, a resonant state, or no state. In the following, we discuss all these scenarios.

For transparency and without loss of generality, we chose to work with the square-well model and study four potentials: repulsive, weakly attractive, moderately attractive, or strongly attractive. The scattering wave function is obtained analytically by solving the stationary Schrödinger equation $-\frac{\hbar^2}{2\mu}\nabla^2\psi + V_0\theta(d-r)\psi = E\psi$, where the reduced mass μ is chosen as 470 MeV, the range parameter d is set at 2.5 fm, and the depth parameter V_0 is set at 25, −10, −25, and −75 MeV for a repulsive potential, a weakly attractive potential not strong enough to generate a bound state, a moderately attractive potential capable of generating a shallow bound state, and a strongly attractive potential yielding a deeply bound state, respectively. We refer to a bound state as a shallow bound state if its binding energy can be described by the effective-range expansion up to q^2, and otherwise as a deeply bound state.

In Fig. 1, panels (a1-d1) show the products of the relative distance r and the S-wave function ψ_0 for the relative momentum $k \simeq 3$ MeV/c. According to Eq. (5), the correlation function depends on two ingredients, namely, the difference between the free and scattering wave functions squared, i.e., $\Delta \equiv r^2(|\psi_0|^2 - |j_0|^2)$, and the source function S_{12}, shown as the blue solid lines and colored regions in panels (a2-d2). As the source size R increases, the magnitude of the Gaussian source function decreases rapidly, and its tail becomes longer, reducing the corresponding correlation function. The final correlation functions are displayed in panels (a3-d3). One can see that (a) for a repulsive

potential, the correlation functions are between zero and unity for different R; (b) for a weakly attractive potential, they are above unity for different R; (c) for a moderately attractive potential, the low-momentum correlation function is above unity for small R while below unity for large R; and (d) for a strongly attractive potential, they are between zero and unity for different R [18].

The above conclusions can also be verified using the momentum space approach in the single-channel case with a potential of the form $V(k) = a + bk^2$, where a and b are (real) low-energy constants (LECs) to be determined. The advantage of this framework is that it can be easily extended to study correlation functions in the presence of virtual or resonant states.

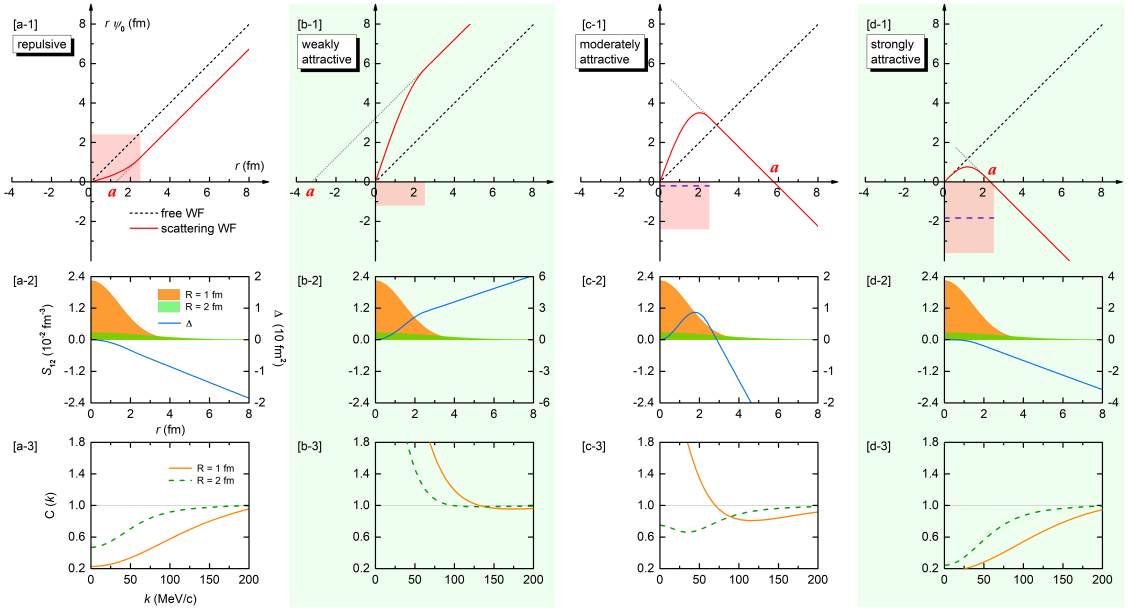

Figure 1: Scattering wave functions, source functions, and correlation functions for the four different square-well potentials, namely, (a) a repulsive potential, (b) a weakly attractive potential, (c) a moderately attractive potential, and (d) a strongly attractive potential [18].

As shown in Fig. 2, for a resonant state characterized by a narrow width (left panels), the correlation function exhibits a pronounced enhancement (peak) at momentum slightly below k_R, where k_R is the center of mass momentum corresponding to the resonance mass. Conversely, a suppression (valley) is observed slightly above k_R. However, for a resonant state characterized by a larger width (middle panels), the peak transforms into an overall enhancement in the low-momentum region, and the valley structure in the high-momentum region becomes less pronounced. In addition, the enhancement and suppression weaken as k_R moves towards the high-momentum region or the source size increases. In the context of virtual states (right panels), the correlation functions consistently exceed unity for varying source sizes, indicating the presence of a purely attractive interaction. Meanwhile, as the virtual-state pole moves away from the threshold, the strength of the attractive interaction decreases, reducing the correlation function.

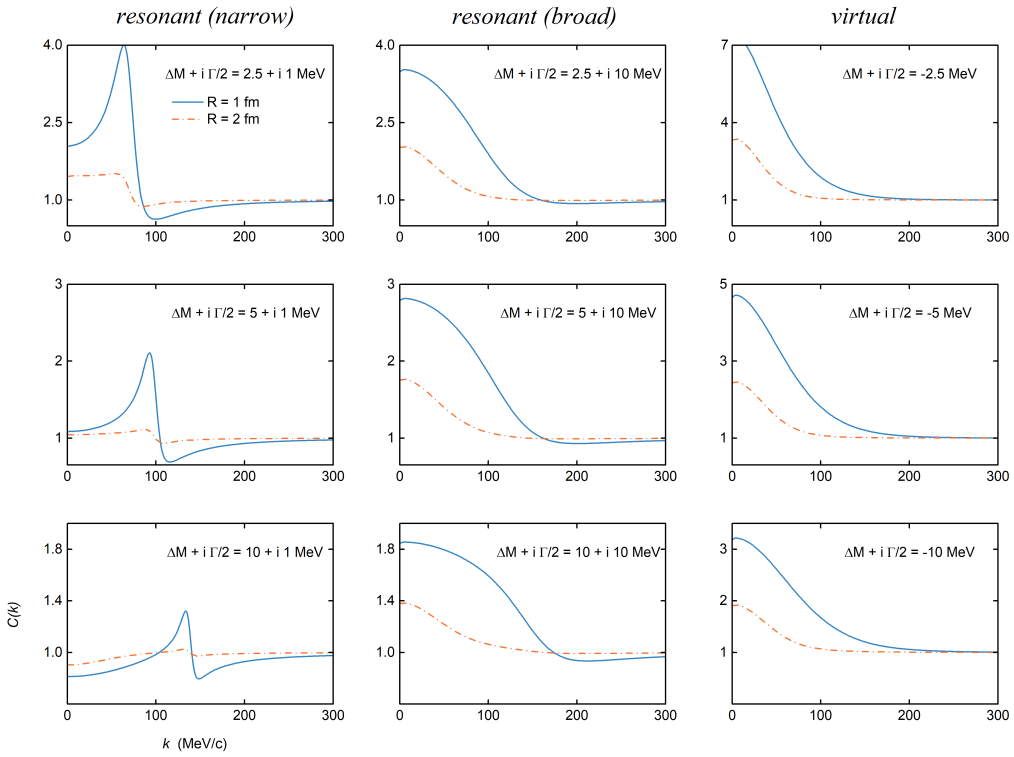

Figure 2: Correlation functions corresponding to potentials capable of generating resonant states with a narrow width (left panels), resonant states with a larger width (middle panels), or virtual states (right panels) with the pole positions $\Delta M + i\Gamma/2$ specified in the respective plots. The source sizes are set at $R = 1$ and 2 fm, and the sharp cutoff $q_{\rm max}$ is fixed to 1 GeV.

4. Selected applications of the femtoscopic technique

4.1 $D_{s0}^*(2317)$ and the DK correlation functions

The $D_{s0}^*(2317)$ has been considered as a bound state of DK and coupled channels [19–22], which is located below the DK threshold by 45 MeV. Therefore, we treat the $D_{s0}^*(2317)$ as a typical deeply bound state. In Ref. [18], we first evaluated the DK coupled-channel interaction in the leading order chiral perturbation theory and then fixed the unknown parameter via reproducing the mass of $D_{s0}^*(2317)$. The corresponding correlation function is shown in Fig. 3. It is found that the inelastic coupled-channel contribution, which is mainly from the $D^0K^+ - D^+K^0$ transition, can be sizable and lead to a cusp-like structure in the D^0K^+ correlation function around the D^+K^0 threshold. We found that the source size dependence of the DK correlation function is very different from that of moderately strong attractive interactions, which can be utilized to verify the nature of $D_{s0}^*(2317)$ as a deeply bound DK state.

4.2 $P_c(4440)$, $P_c(4457)$, and the $\bar{D}^*\Sigma_c$ correlation functions

The spins of the two pentaquark states $P_c(4440)$ and $P_c(4457)$ can help distinguish various theoretical interpretations [12]. Recently, we proposed to discriminate the spins of $P_c(4440)$ and $P_c(4457)$ with the femtoscopic technique [23]. Assuming $P_c(4440)$ and $P_c(4457)$ are $\Sigma_c\bar{D}^*$ bound

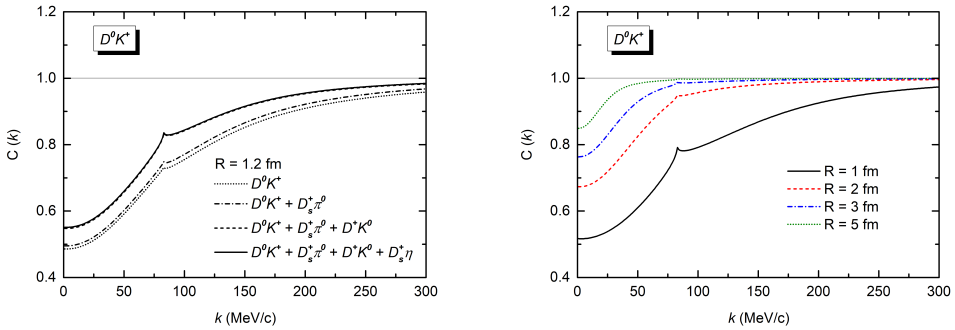

Figure 3: (Left panel) D^0K^+ correlation function as a function of the relative momentum k. The results are calculated with the LO chiral potential and a Gaussian source of $R = 1.2$ fm. (Right panel) Source size dependence of the D^0K^+ correlation function. .

states, we first evaluated their interactions without specifying their spin by reproducing the masses of $P_c(4440)$ (strongly attractive) and $P_c(4457)$ (moderately attractive) in the resonance saturation model. Then, we calculated the corresponding $\Sigma_c^+\bar{D}^{*0}$ correlation functions. In Fig. 4, the $\Sigma_c\bar{D}^*$ correlation functions C_s (C_m) calculated with the moderately (strongly) attractive interactions are in remarkable agreement with the aforementioned general features of correlation functions, namely, a moderately attractive interaction and a strongly attractive one may result in entirely different low-momentum behavior. The spin-averaged $\Sigma_c\bar{D}^*$ correlation functions and their source size dependence are also shown in Fig. 4. The low-momentum behavior of the spin-averaged results is pretty different in the two spin assignments, especially for a small collision system, which can be used to determine the spins of $P_c(4440)$ and $P_c(4457)$. In addition, we suggest using the source size dependence of the $\Sigma_c^+\bar{D}^0$ correlation function to determine the source size of $\Sigma_c^+\bar{D}^{*0}$.

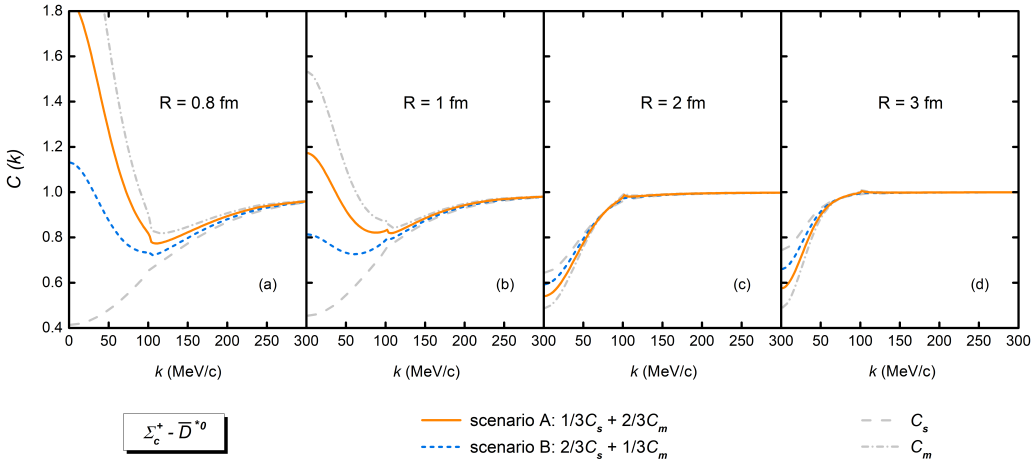

Figure 4: Spin-averaged $\Sigma_c^+\bar{D}^{*0}$ correlation function as a function of the relative momentum k for different source sizes $R = 0.8, 1, 2$ and 3 fm, respectively. The blue short-dashed lines represent the spin-averaged results in scenario A, where $P_c(4440)$ and $P_c(4457)$ have $J^P = (1/2)^-$ and $J^P = (3/2)^-$ respectively, while the orange solid lines represent the results in scenario B where $P_c(4440)$ and $P_c(4457)$ have $J^P = (3/2)^-$ and $J^P = (1/2)^-$. For reference, the $\Sigma_c^+\bar{D}^{*0}$ correlation functions calculated with the moderately (strongly) attractive interactions without specified spin are also shown as the dash-dotted (dashed) lines.

4.3 $Z_c(3900)$, $Z_{cs}(3985)$, and the $D\bar{D}^*$ and $D\bar{D}_s^*$ correlation functions

The $Z_c(3900)$ and $Z_{cs}(3985)$ are often interpreted as the $D\bar{D}^*$ and $D\bar{D}_s^*$ resonant states from the experimental analyses based on the Breit-Wigner parametrization [8, 9]. However, various theoretical re-analyses of the same data suggest they can be either resonances or virtual states [24]. Recently, we demonstrated that the femtoscopic technique can help determine whether $Z_c(3900)$ and $Z_{cs}(3985)$ are resonances or virtual states [25].

In Ref. [25], we first evaluated the $D^0D^{*-}/D^0D_s^{*-}$ interactions by precisely reproducing the pole positions of $Z_c(3900)/Z_{cs}(3985)$ in the resonant and virtual state scenarios, respectively. Subsequently, we computed the corresponding $D^0D^{*-}/D^0D_s^{*-}$ correlation functions.

As depicted in Fig. 5, the $D^0D_s^{*-}$ correlation function exhibits a pronounced enhancement in a wide range of the relative momentum k in the virtual state scenario. Conversely, in the resonant state scenario, the D^0D^{*-} correlation function remains enhanced in the low-momentum region but exhibits a suppression in the high-momentum region. This feature serves as a crucial criterion in distinguishing between the two scenarios. In addition, as the source size R decreases, the difference in the correlation functions between these two scenarios becomes more pronounced, reflecting the short-range nature of the strong interaction.

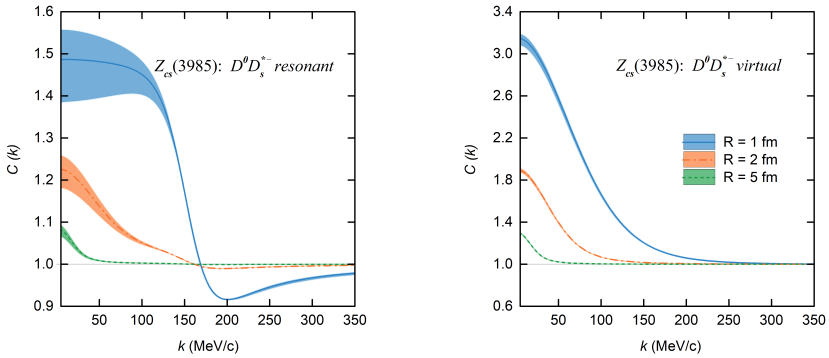

Figure 5: $D^0D_s^{*-}$ correlation function as a function of the relative momentum k for different source sizes R = 1, 2, and 5 fm. The results are obtained with the energy-dependent potential, which describes the $Z_{cs}(3985)$ as a resonant state, and with the constant contact-range potential, which interprets the $Z_{cs}(3985)$ as a virtual state. The bands reflect the sharp cutoff variation, $q_{\rm max}$ = 0.8 − 1.2 GeV.

5. Summary and outlook

The femtoscopic technique can be powerful in extracting the strong interactions among stable and unstable hadrons and, therefore, can be utilized to understand the nature of many exotic hadrons discovered. So far, its potential has not yet been fully explored. Given the large statistics achievable in the LHC run 3, in particular, more experimental and theoretical efforts are strongly encouraged to better understand the source function and three-hadron correlation functions.

6. Acknowledgments

This work is partly supported by the National Key R&D Program of China under Grant No. 2023YFA1606700 and the National Science Foundation of China under Grant No. 12435007.

References

[1] E. Rutherford, Philosophical Magazine, Series 6, 1911, 21 (125): 669.

[2] L. Fabbietti, V. Mantovani and O. Vazquez Doce, Ann. Rev. Nucl. Part. Sci. 71 (2021) 377.

[3] M. Gell-Mann, Phys. Lett. 8 (1964) 214.

[4] G. Zweig, CERN-TH-401, 1964.

[5] S. K. Choi and et al., Phys. Rev. Lett. 91 (2003) 262001.

[6] B. Aubert and et al. (BaBar Collaboration), Phys. Rev. Lett. 90 (2003) 242001.

[7] D. Besson and et al. (CLEO Collaboration), Phys. Rev. D 68 (2003) 032002.

[8] M. Ablikim and et al. (BESIII Collaboration), Phys. Rev. Lett. 110 (2013) 252001; Phys. Rev. Lett. 126 (2021) 102001.

[9] Z. Q. Liu and et al. (Belle Collaboration), Phys. Rev. Lett. 110 (2013) 252002.

[10] R. Aaij and et al. (LHCb Collaboration), Phys. Rev. Lett. 115 (2015) 072001; Phys. Rev. Lett. 122 (2019) 222001.

[11] S. Navas and et al. (Particle Data Group Collaboration), Phys. Rev. D 110 (2024) 030001.

[12] M. Z. Liu, Y. W. Pan, F. Z. Peng, M. Sánchez Sánchez, L. G. Geng, A. Hosaka and M. Pavon Valderrama, Phys. Rev. Lett. 122 (2019) 242001.

[13] T.W. Wu, Y. W. Pan, M. Z. Liu and L. S. Geng, Sci. Bull. 67 (2022) 1735.

[14] M. Z. Liu, Y. W. Pan, Z. W. Liu, T. W. Wu, J. X. Lu and L. G. Geng, arXiv 2404.06399.

[15] S. E. Koonin, Phys. Lett. B 70 (1977) 43.

[16] R. Lednicky and V. L. Lyuboshits, Yad. Fiz. 35 (1981) 1316.

[17] S. Pratt, T. Csorgo and J. Zimanyi, Phys. Rev. C 42 (1990) 2646.

[18] Z. W. Liu, J. L. Lu and L. G. Geng, Phys. Rev. D 107 (2023) 074019.

[19] E. E. Kolomeitsev and M. F. M. Lutz, Phys. Lett. B 582 (2004) 39.

[20] F. K. Guo, P. N. Shen, H. C. Huan, Phys. Lett. B 647 (2007) 133.

[21] D. Gamermann, E. Oset, D. Strottman and M. J. Vicente Vacas, Phys. Rev. D 76 (2007) 074016.

[22] M. Altenbuchinger, L. S. Geng and W. Weise, Phys. Rev. D 89 (2014) 014026.

[23] Z. W. Liu, J. L. Lu, M. Z. Liu and L. G. Geng, Phys. Rev. D 108 (2023) L031503.

[24] M. L. Du, M. Albaladejo, F. K. Guo and J. Nieves, Phys. Rev. D 105 (2022) 074018.

[25] Z. W. Liu, J. L. Lu, M. Z. Liu and L. G. Geng, arXiv 2404.18607.